Icarus 320 (2019) 49–59

Contents lists available at ScienceDirect

Icarus

journal homepage: www.elsevier.com/locate/icarus

Tectonic analysis of fracturing associated with occator crater

Debra L. Buczkowski[a,*], Jennifer E.C. Scully[b], Lynnae Quick[c], Julie Castillo-Rogez[b], Paul M. Schenk[d], Ryan S. Park[b], Frank Preusker[e], Ralf Jaumann[e], Carol A. Raymond[b], C.T. Russell[f]

[a] Johns Hopkins Applied Physics Laboratory, 11100 Johns Hopkins Rd., Laurel, MD 20723, USA
[b] NASA Jet Propulsion Laboratory, California Institute of Technology, 4800 Oak Grove Dr., Pasadena, California 91109, USA
[c] Smithsonian Institute, 10th St. & Constitution Ave. NW, Washington DC 20560 USA
[d] Lunar and Planetary Institute, 3600 Bay Area Blvd., Houston, Texas 77058, USA
[e] German Aerospace Center (DLR), Rutherfordstrasse 2, Berlin 12489, Germany
[f] University of California, Los Angeles, 405 Hilgard Ave., Los Angeles, California 90095, USA

ARTICLE INFO

Article history:
Received 19 September 2017
Revised 14 May 2018
Accepted 14 May 2018
Available online 21 May 2018

ABSTRACT

Occator crater, a Ceres crater that hosts multiple bright spots on its floor, has several sets of fractures associated with it. A tectonic analysis of each of these fracture sets suggests that the concentric and radial fractures around the central pit and the concentric fractures high on the crater wall (near the rim) most likely formed due to well known impact cratering processes. Uplift of the crater floor due to magmatic injection is suggested to have resulted in the concentric floor fractures at the base of the crater wall, as well as the cross-cutting fractures in the lower part of the southwestern wall. A mathematical analysis shows that a cryomagmatic plume (diapir) could have both reached the height necessary to cause fracturing within Occator, and that the stresses required are reasonable. Expansion a lobate flow from beneath is proposed to have formed those linear fractures associated with the Vinalia Faculae. Circumferential fractures surrounding Occator appear to have formed due to the volumetric compaction of the ejecta blanket over the buried pre-existing topography.

1. Introduction

NASA's Dawn spacecraft (Russell and Raymond, 2011) was captured into Ceres orbit on March 6, 2015. On board was the Framing Camera (FC) (Sierks et al., 2011), which provided the first images of Ceres' surface. Observation of these FC data discovered that the feature originally identified in Hubble Space Telescope data as "Bright Spot 5" (Li et al., 2006) is actually comprised of multiple bright spots on the floor of Occator crater (Nathues et al., 2015).

Occator crater is a 92 km diameter crater located at 19.8°N, 239.3°E on Ceres (Fig. 1). Similar to the larger craters found on the icy moons Ganymede and Callisto (Schenk, 1993), Occator has a pit and dome complex at the crater center (Schenk et al., 2016). The floor of Occator is cut by multiple sets of linear fractures, while concentric fractures are found on both the crater floor, around the central pit, on the crater walls, and in the ejecta (Fig. 1c). The bright spots now named the Vinalia Faculae are noticeably associated with floor fractures (Buczkowski et al., 2016), while the brightest spot, Cerealia Facula, is associated with the central pit (Nathues et al., 2015) (Fig. 1a).

Occator crater is found on Hanami Planum, the highest standing region on Ceres (Buczkowski et al., 2016). Hanami is one of the regions of Ceres that has a strong gravity anomaly (Ermakov et al., 2017). One possible explanation for the high topography but negative Bouguer gravity anamoly was found to be a combination of a buoyancy-driven anomaly and a thicker crust, although an anomalously low crustal density in the region could also account for it (Ermakov et al., 2017). Analysis of the Samhain Catenae, a series of faults also located on Hanami Planum, suggest that the crust in this region is 58 km in thickness (Scully et al., 2017), consistent with the maximum gravity-based crustal thickness prediction of 52.7 km (Ermakov et al., 2017).

We have created a fracture map of Occator crater using ESRI ArcGIS 10.3 software. A Framing Camera (FC) Low Altitude Mapping Orbit (LAMO – 35 m/px) clear image mosaic was used as a basemap. We also utilized a global digital terrain model (DTM) derived from High Altitude Mapping Orbit (HAMO - 140 m/px) stereo images with vertical accuracy of ~15 m and spatial resolution of ~140 m/pixel (Preusker et al., 2016), as well as an Occator specific

* Corresponding author.
E-mail address: Debra.Buczkowski@jhuapl.edu (D.L. Buczkowski).

https://doi.org/10.1016/j.icarus.2018.05.012
0019-1035/

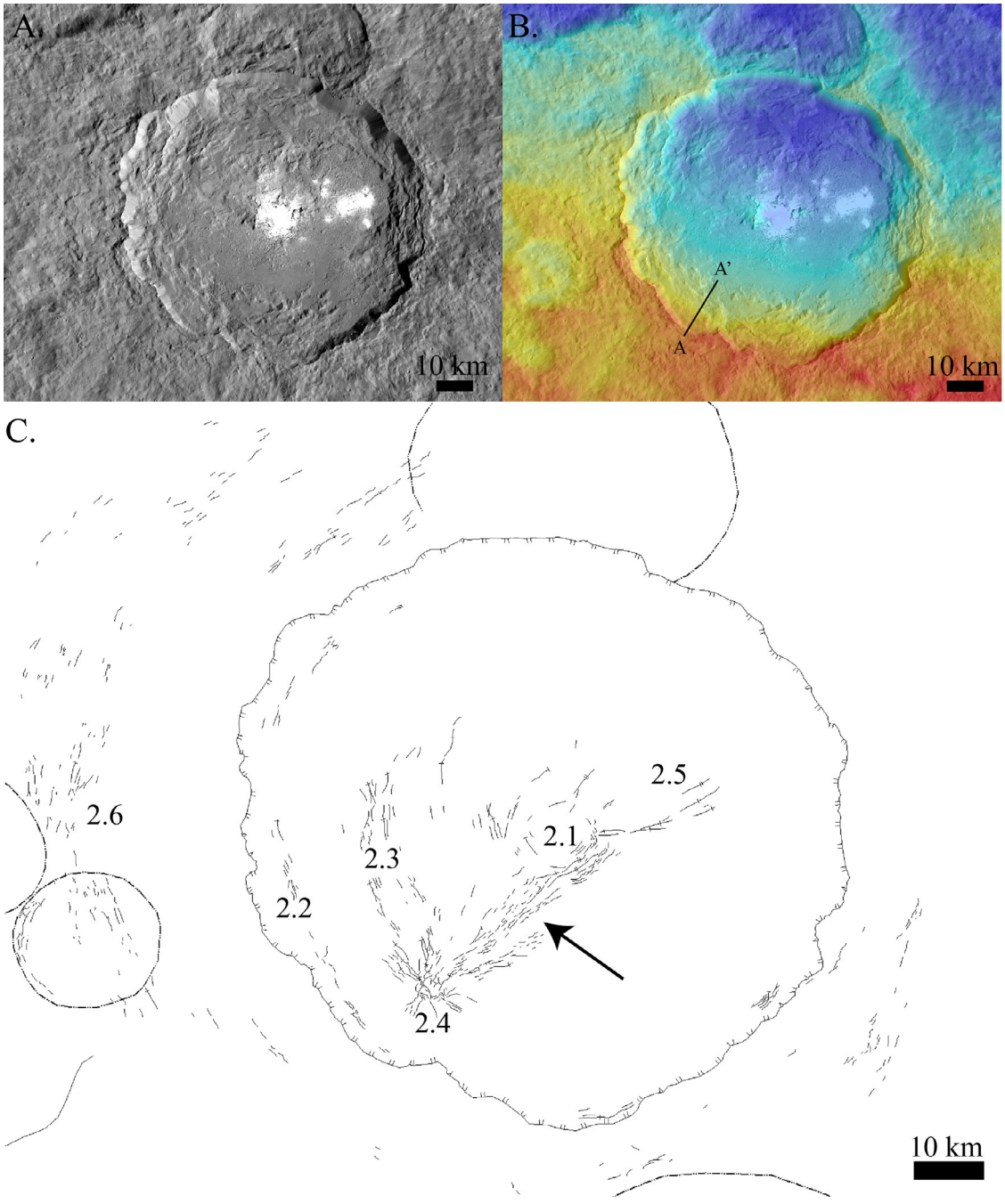

Fig. 1. A) LAMO mosaic of Occator crater and surrounding ejecta. B) HAMO topography of same area. C) Fracture map of region, showing fractures on the floor of Occator, in the crater walls, and in the surrounding ejecta. Numeric labels refer to the subsection of the paper that discusses the associated fractures.

LAMO DTM with vertical accuracy of ~1.5 m and spatial resolution of ~35 m/pixel (Jaumann et al., 2017).

Occator is only one of several floor-fractured craters (FFCs) observed on Ceres (Buczkowski et al., 2016). The morphology of these Ceres FFCs have been compared to lunar FFC morphology and it has been suggested that they may share similar formation mechanisms (Buczkowski et al., 2016). However, a topographic, morphologic and structural analysis of Occator suggests that not all of its fracture sets formed due to FFC formation processes.

2. Fracture sets

Occator crater has several sets of fractures associated with it (Fig. 1), including: 1) Concentric and radial fractures around the central pit; 2) Concentric floor fractures at the base of the crater wall; 3) Concentric fractures high on the crater wall, near the crater rim; 4) Cross-cutting fractures in the lower part of the southwestern wall; 5) Linear fractures associated with the Vinalia Faculae; and 6) Circumferential fractures in the ejecta blanket. We have performed a tectonic analysis of each of these sets of fractures, and have determined the formation mechanism for each.

2.1. Pit fractures

2.1.1. Descripton

Occator crater does not have a central peak, but rather has a 9 km diameter, 1 km deep central pit (Fig. 2a and b) with an uplifted dome on its floor (Fig. 2c) (Hiesinger et al., 2016). There is

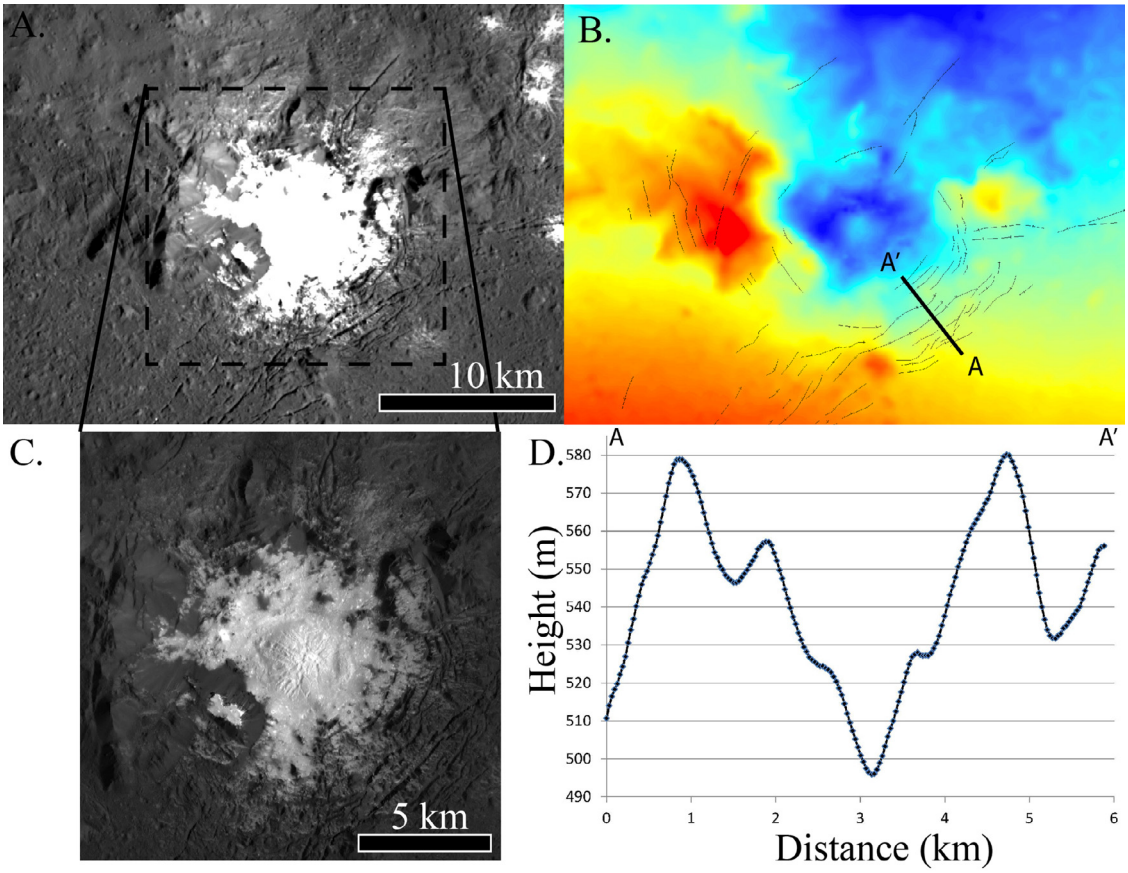

Fig. 2. Fractures associated with the Occator central pit. A) LAMO (35 m/pixel) clear filter image of the central pit and associated fractures. To best view the structures, Ceralia Facula had to be overexposed, hiding the floor of the pit. Dashed square shows location of part (c). B) LAMO DTM of the central pit, with map of the associated structures. A to A' line shows location of profile shown in part (d). C) LAMO image of the central pit stretched to allow viewing of the dome on the floor of the pit. D) Topographic profile across multiple pit structures. The raw profile is dominated by the downward slope of the central pit; the profile shown has thus been detrended.

an extensive set of concentric fractures around this central pit, as well as a smaller number of radial fractures (Fig. 2b). The concentric fractures are found 360° around the central pit, starting at 4.1 km from the center of the pit to the north and southeast, and extending outward as much as 13.1 km from the center of the pit to the west. Fracture depth ranges from 30 – 80 m (Fig. 2d) while length ranges from 1–7 km. The fractures are v-shaped, with no topographic evidence of fault slip (Fig. 2d).

Radial fractures extend up to 5 km away from the concentric fractures, to the north, east and southwest of the pit. They are less deep than the concentric fractures, with depths ranging from 13–42 m, but have the same v-shaped morphology.

In addition to the fractures outside of the pit, there are cross-cutting fractures on the surface of the dome on its floor (Fig. 2c). The depth of these fractures is below the level of resolution of even the LAMO DTM. However, the pattern of fracturing (Fig. 2c) strongly resembles fracture systems that form in physical analog models of domal uplift (e.g. Schultz-Ela et al., 1993; Sims et al., 2013) and are observed on terrestrial salt domes (e.g. Bosak et al., 1998; Sims et al., 2013).

2.1.2. Interpretation

Lunar floor-fractured craters (Schultz, 1976) frequently have both radial and concentric fractures around their central peaks, thought to form due to doming of the crater center due to magmatic intrusion and laccolith formation beneath the crater (Jozwiak et al., 2015). But while the Occator pit fractures could be a result of increased bending stresses due to floor doming, it is also possible that they simply formed as a result of the collapse of the pit itself.

Many of the large (>60 km) craters on the icy moons Ganymede and Callisto have central pits with interior domes, instead of central peaks (Schenk, 1993). It is thought that the icy composition of the target material is a factor in pit formation, which is consistent with the observation of similar pit craters on icy Ceres (Schenk et al., 2016). There have been several proposed formation mechanisms for these pits, including 1) surface collapse into a void left by the release of volatiles due to impact into an ice-rich target (Wood et al., 1978; Tornabene et al., 2007), 2) surface collapse because of a mechanically weaker layer at shallow depth (Greeley et al., 1982; Schenk, 1993), or 3) central uplift collapse and drainage of impact melt into sub-crater fractures (Bray et al., 2012). The similarity of the morphology of the Occator pit and dome to those seen in impact craters on Ganymede and Callisto implies that similar mechanisms may be operating on these three bodies (Schenk et al., 2016). Any of the proposed methods of pit collapse would result in radial extensional stresses which could trigger the concentric fracturing we see around Occator's central pit. Since according to these models pit collapse would be a part of impact crater formation, this would mean that this fracturing occurred during the formation of Occator.

It has been suggested that the domes inside the central pits of craters on Ganymede and Callisto are not domical uplifts per se, but rather exposures of a compositionally distinct subsurface layer that was mobilized and exposed during the impact event (Schenk, 1993). However, this proposed process of dome formation likely would not result in the fracture pattern found on the

dome observed in Occator (Fig. 2c), since it is most consistent with formation by domal uplift and the driving force proposed by Schenk (1993) was inertia. Quick (2018) proposed that the Cerealia dome could have formed due to cycles of diapiric intrusion and lava extrusion, similar to how lava domes form on the Earth. While terrestrial lava domes can have fractures in patterns similar to those observed on the Ceralia dome, the observed fracture pattern is more consistent with domes formed due to uplift (e.g. Schultz-Ela et al., 1993, Bosak et al., 1998; Sims et al., 2013). A formation mechanism for the Ceralia dome such as the buoyancy-driven diapir of subsurface material proposed for dome formation on Ganymede by Moore and Malin (1988) could explain not only the fracture set on the apex of the dome, but also the relatively young Cerealia Facula deposit associated with it (e.g. Stein et al., 2017; Quick, 2018; Schenk et al.,2018; Scully et al., 2018).

2.2. Concentric fractures near the crater rim

2.2.1. Description

Small-scale fractures are identified high on the Occator's crater wall, circumferential (but interior) to the crater rim (Fig. 3). These fractures range in length from 1–4 km, depths from 1–7 m, and are up to 300 m wide. Talus deposits from higher on the crater wall cover these fractures at many locations within Occator (Fig. 3d).

2.2.2. Interpretation

The wall of Occator is heavily terraced (Buczkowski et al., 2016), and all of these fractures are located within the geologic unit "crater terrace material" (Scully et al., 2018). According to crater formation models, crater terraces are interpreted to form due to downward movement along a series of concentric faults that formed during impact crater formation during the collapse of the transient crater (French, 1998). The orientation and location of the observed small-scale fractures on the Occator wall suggest that they may have also formed during this transient crater collapse, but without any accompanying displacement of the wall material. Talus materials from higher on the crater wall completely cover these rim fractures, supporting the idea that the fractures formed during impact crater formation, not at some later date. Similar undisplaced crater terrace fault traces have been observed in craters on Mars (Collins, 2014) that also display ice-related morphologies such as pingos (Dundas et al., 2008), suggesting that these features might be indicative of cratering into ice-rich regolith.

2.3. Concentric floor fractures at the base of the crater wall

2.3.1. Description

Small-scale fractures are also found at the base of the western crater wall of Occator (Fig. 4). These particular concentric fractures are only found for ~90° around the base of the Occator wall, extending from due west down to the southwest. Compared to the pit fractures, these fractures are relatively shallow (5–10 m deep) although they are comparable in length (2.5–3.5 km). However, unlike either the pit fractures or the rim fractures, they have flat floors and show some signs of a small amount of fault displacement (<10 m) (Fig. 4c).

2.3.2. Interpretation

Ceres FFCs have been cataloged according to the lunar classification scheme (Jozwiak et al., 2015). Occator is most consistent with Type 1 lunar FFCs, having a central peak/pit complex, wall terraces, and both radial and concentric fractures (Buczkowski et al., 2016). Other large (>50 km) Ceres FFCs are also consistent with Type 1 lunar FFCs, while smaller craters on

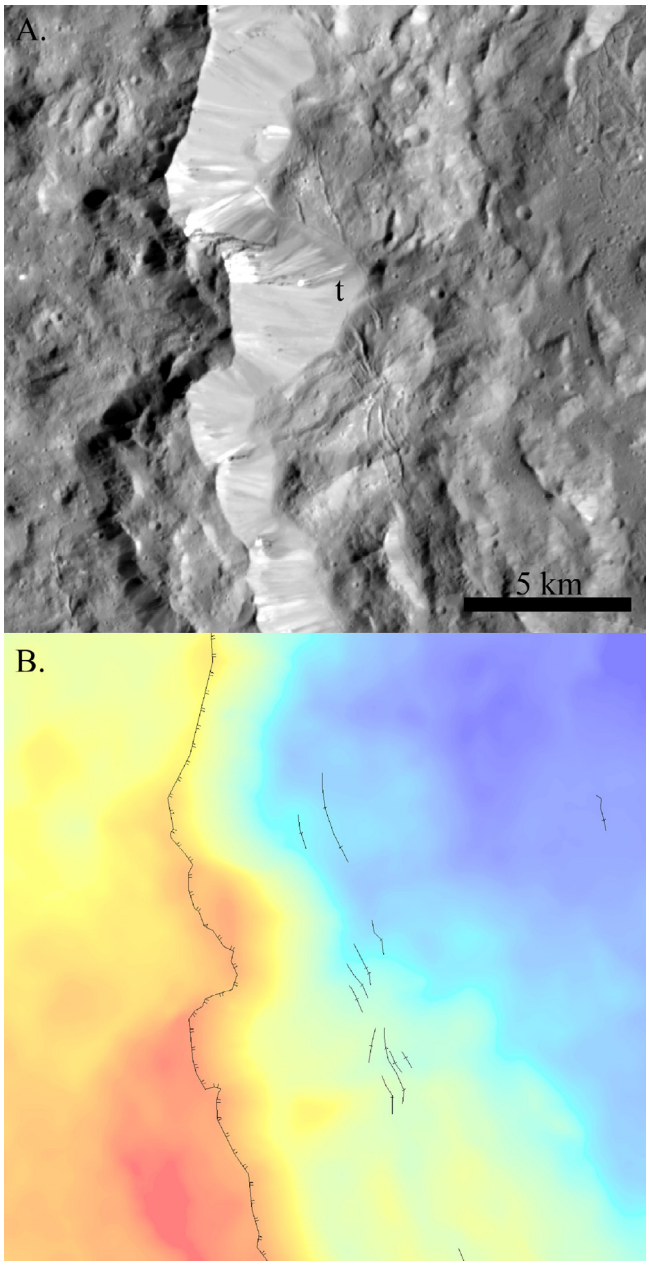

Fig. 3. Concentric fractures high on the crater wall. A) LAMO (35 m/pixel) clear filter image of the concentric fractures found on the western Occator wall, just below the crater rim. Letter "t" shows where talus deposit completely covers fractures. B) Fracture map of the same area, shown over the LAMO DTM of Occator crater.

Ceres are more consistent with Type 4 lunar FFCs, having less-pronounced floor fractures and a v-shaped moats separating the wall scarp from the crater interior (Buczkowski et al., 2016).

Like the other Ceres FFCs, Occator is anomalously shallow compared to non-fractured Ceres craters (Buczkowski et al., 2016). This is consistent with lunar FFCs (Jozwiak et al., 2012, 2015) and suggests that the floor fractures may be due the intrusion of a low-density material uplifting the floor. On the Moon this material is assumed to be basaltic magma (Jozwiak et al., 2012, 2015), but given the low density of Ceres, basalt is unlikely to be present. However, it has been determined that a cryomagma composed of a mixture of water ice, chloride-rich brines, and secondary minerals such as carbonates and phyllosilicates is likely to be present on Ceres (Neveu and Desch, 2015; Ruesch et al., 2016). This cryomagma could potentially be the low-density material uplifting the

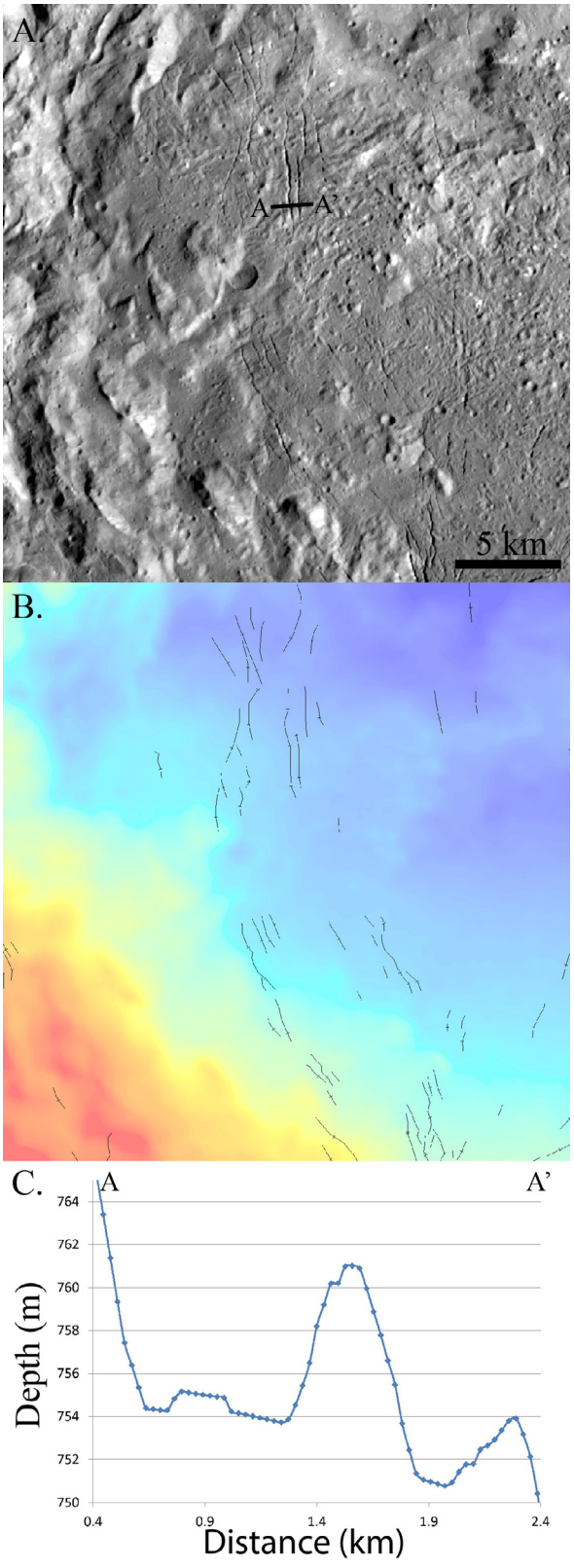

Fig. 4. Concentric fractures at the base of the crater wall. A) LAMO (35 m/pixel) clear filter image of the concentric fractures found on the western Occator wall. Line labeled A-A' indicates the location of the topographic profile shown in part c. B) Fracture map of the same area, shown over the LAMO DTM of Occator crater. C) Topographic profile of sample concentric fractures. Location shown in part A.

Occator floor and creating the observed fractures. The association of the fractures with the high albedo, sodium carbonate-bearing Vinalia Faculae, supports the involvement of cryomagma in fracture formation (Buczkowski et al., 2016; Stein et al., 2017; Quick ,2018; Ruesch et al., 2018).

Models for fracture formation in lunar FFCs invoke a piston-like uplift of the entire crater floor as the last stage of magmatic intrusion beneath the crater (Jozwiak et al., 2015). This localizes bending stresses at the periphery of the intrusion, which results in concentric fracturing and faulting adjacent to the crater wall (Jozwiak et al., 2015). This orientation is similar to what is observed in this set of Occator fractures, suggesting that these particular Occator fractures were formed during an advanced stage of magmatic intrusion beneath the crater. However, the fact that these fractures are only present in the southwest portion of the crater suggests that only this part of the crater would have undergone the proposed piston-like uplift.

A quantitative analysis of whether or not a Ceres cryomagma could uplift the crater floor of Occator and create the observed fracture systems is explored in the Discussion section of this paper.

2.4. Cross-cutting fractures in the SW wall

2.4.1. Description

An arrangement of fractures (Fig. 5a) found at the base of the SW Occator wall are located in the region of concentric floor fractures, but have a pattern of cross-cutting fractures that is more consistent with that observed to occur due to domal uplift (e.g. Schultz-Ela et al., 1993, Bosak et al., 1998; Sims et al., 2013). These fractures show apparent broad outer arc extension, with at least two axes of fracturing (Fig. 5b). A transition to radial faulting occurs with distance from the fracture axes; this is consistent with the change in stress orientation that occurs at the edge of all domes.

A topographic profile down the slope of the Occator crater wall (Fig. 6a) shows that there is a flat-topped dome at the location of the fracture set (Fig. 6b). The fractures associated with the major fracture axis ("x" in Fig. 5b) have depths ranging from 61–97 m and widths ranging up to 2.2 km (Fig 6c); they extend anywhere from 6 - 7.5 km from the center of fracturing. The fractures associated with the smaller axis ("y" in Fig. 5b) are not quite as deep (23–36 m) or as wide (0.8–1.2 km) (Fig 6c), and their lengths are more variable, ranging from 1.1 to 5.5 km from the center of fracturing. While some of the fractures are v-shaped, several have flat floors and evidence of displacement along the wall, suggesting faulting has occurred (Fig. 6c).

Fractures from both axes cut through wall terrace material, suggesting that both sets of fractures formed some time after the collapse of the transient crater during impact crater formation. However, fractures extending from the minor axis **y** abut against fractures associated with the major axis, suggesting that the minor axis represents a later incident of doming and associated fracturing.

A set of linear fractures on the Occator floor occur between the SW wall fracture set and the central pit (black arrow, Fig. 1c). It is possible that these linear fractures are simply linkages of those fractures radial to the fractures associated with doming and those fractures radial to the central pit.

2.4.2. Interpretation

In lunar FFCs, magma can utilize the concentric fractures at the base of the crater wall to travel to the surface (Jozwiak et al., 2015). In lunar FFCs this usually results in either mare or pyroclastic deposits forming on the surface near the fracture.

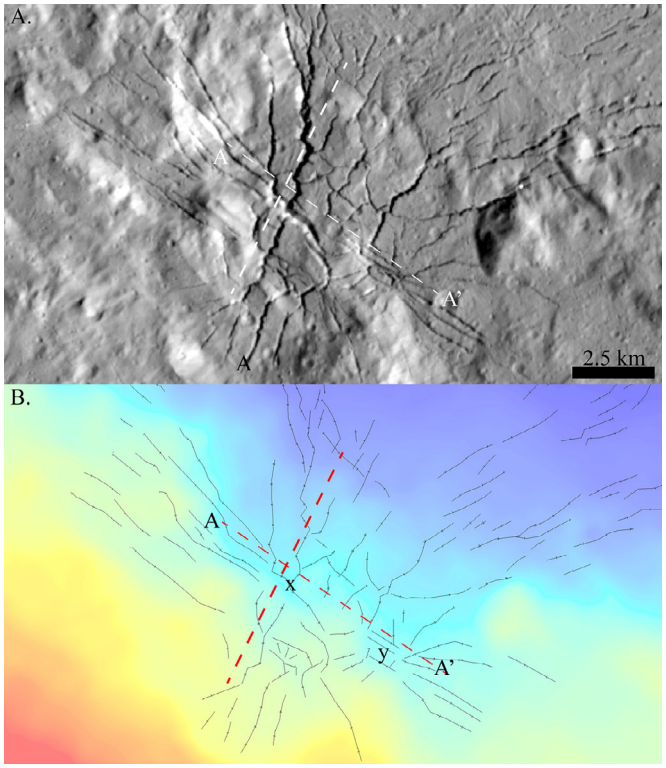

Fig. 5. Crosscutting fractures at the base of the southwestern crater wall. Dashed line A-A' showslocation of topographic profile shown in Fig. 6c. Unlabled dashed line shows the part of the topographic profile shown in Fig. 6b. A) LAMO (35 m/pixel) clear filter image of the crosscutting fractures found on the southwestern Occator wall. B) Fracture map of the same area, shown over the LAMO DTM of Occator crater. Major axis of fracturing is noted by a "x" while the minor axis of fracturing is noted by a "y".

There is no evidence of either lava flows or pyroclastic deposits associated with these fractures (Buczkowski et al., 2016). However, it is possible that if upward-moving cryomagma utilized the fracturing associated with piston uplift of the Occator floor it would result in a localized doming event, similar to laccolith formation, instead of reaching the surface as a flow or explosive deposit. Such doming would result in fracturing of the surface, and physical analog models (e.g. Schultz-Ela et al., 1993, Sims et al., 2013) show that the expected pattern would be similar to the one observed.

2.5. Linear fractures associated with vinalia faculae

2.5.1. Description

While much of the southern floor of Occator is covered by relatively flat, knobby to smooth material that could very well be impact melt (Hiesinger et al., 2016; Schenk et al., 2016, this issue; Scully et al., 2018), in northeast Occator is a morphologically distinct floor material (Fig. 7). This material has well-defined lobate margins extending away from the center of the crater (Buczkowski et al., 2016), and has been interpreted to be a cryovolcanic flow (Krohn et al., 2016). To the south the flow stands 160 m higher than the rest of the crater floor materials (Fig. 8a), while it is 241 m higher than floor materials at the base of the crater wall (Fig. 8b). The surface of the flow has a ropy, hummocky texture somewhat similar to what is observed on the floor of Class 4 Ceres FFCs (Buczkowski et al., 2016); the topography of this hummocky texture is very similar to that of the fractures (Fig. 8), although the visible morphology is noticeably different (Fig. 7).

Linear structures cross the southern part of the lobate flow and are roughly radial to the crater's central pit. The fractures are v-shaped in morphology and can be quite shallow, with depths averaging at ~10 m although the deepest fracture reaches 33 m; they vary in length from 1.8 to 7.2 km and they tend to be ~1 km wide. There is a strong spatial association between these fractures and the Vinalia Faculae (Fig. 7a), high-albedo deposits with wispy margins that are composed of sodium carbonate (De Sanctis et al, 2016).

To the south of the lobate flow are a small number of fractures concentric to the crater wall (Fig. 7b). Unlike the concentric frac-

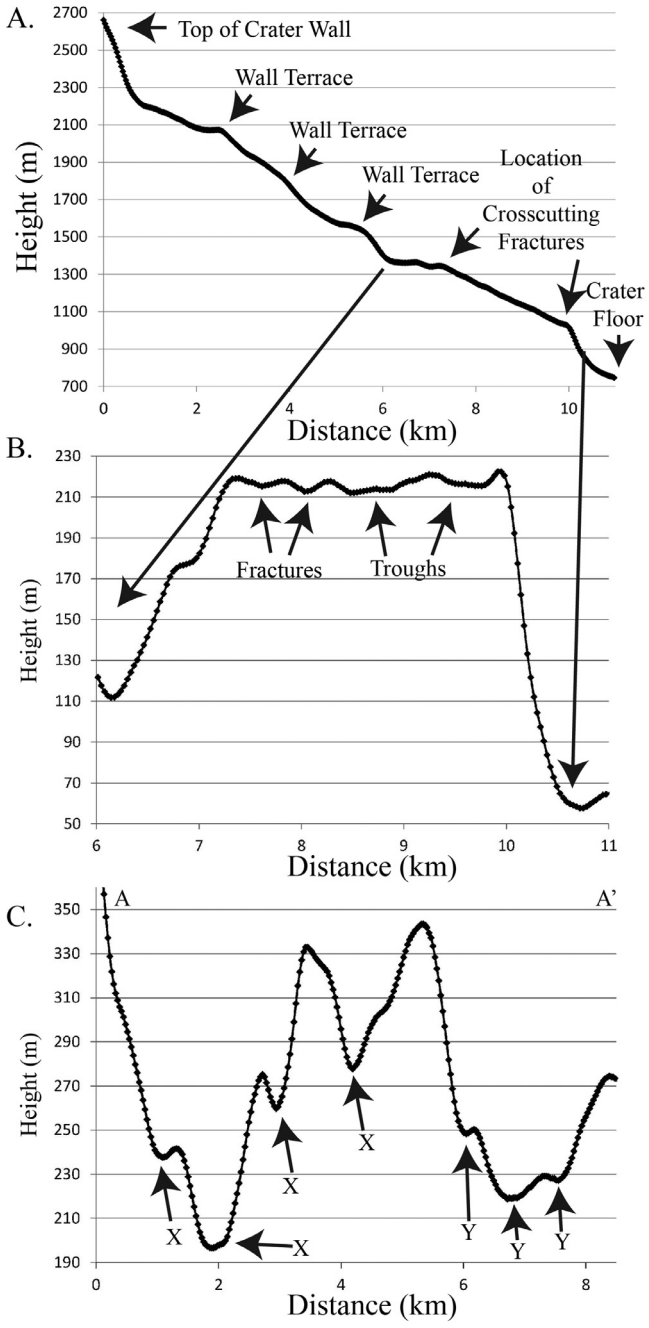

Fig. 6. Topographic profiles of crosscutting fractures at the base of the southwestern crater wall. A) Profile of Occator wall, from the crater rim, through the major axis of fracturing X (noted in Fig. 5). Location of major features, such as the top of the crater wall, the beginning of the crater floor, various crater terraces, and the location of the cross-cutting fractures (which is a subtle dome-like structure) are noted. Profile line is shown in Fig. 1b. B) Profile of the location of the cross-cutting fractures is shown, with the downward slope of the crater wall removed. A noticeable dome-shaped feature is revealed. C) Topographic profile across the major axes of fracturing. Profile line is shown in Fig. 5b. Fractures and troughs are labeled with X or Y to note which set of fractures they are associated with.

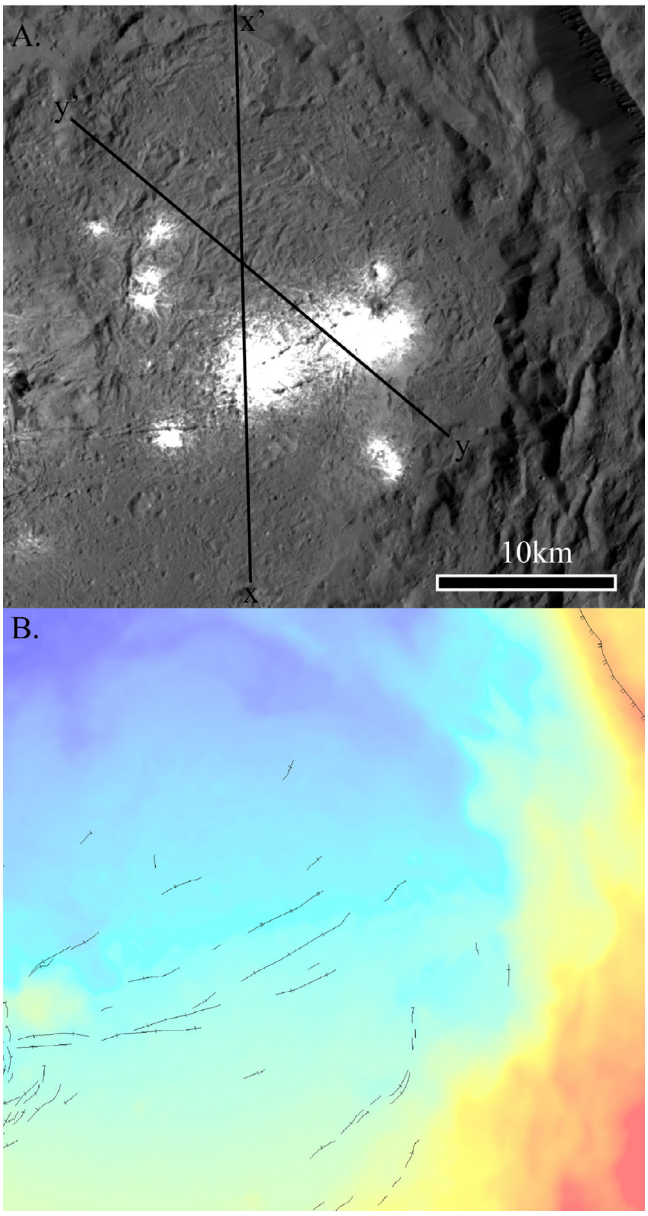

Fig. 7. Linear fractures on lobate flow on crater floor. Topography of profiles X–X' and Y–Y' are shown in Fig. 8. A) LAMO (35 m/pixel) clear filter image of the lobate flow found on the northeastern Occator floor. B) Fracture map of the same area, shown over the LAMO DTM of Occator crater.

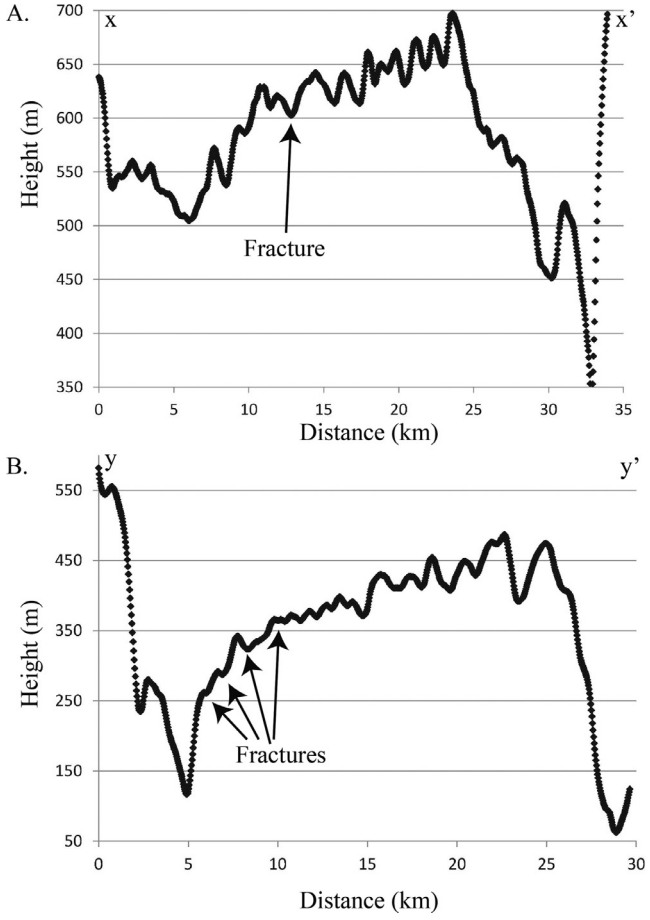

Fig. 8. Topographic profiles of lobate flow on northeastern Occator floor (location shown in Fig. 7). Northward slope is removed to accentuate surface structures. A) Profile of lobate flow from south to north, starting at crater materials that cover most of the Occator and going over the lobate flow. The ropy surface of the flow resembles fractures; the profile crosses only one major fracture, which is labeled. B) Profile of lobate flow from east to west, starting at the base of the crater wall and going over the lobate flow. The profile crosses four major fractures, which are labeled.

tures discussed in Section 2.3, these concentric fractures are associated with a bright Vinalia Facula deposit (Fig. 7a).

2.5.2. Interpretation

The ropy, hummocky texture of the lobate flow in Occator is reminiscent of that of lava flows on Earth that have undergone inflation. Inflation occurs when the surface crust of the flow cools but the underlying liquid volume increases in size due to high effusion rates and sustained lava injection (Hon et al., 1994). This can result in uniform uplift of the entire flow sheet. Inflation fractures can form as pressure within a lava flow induces circumferential stress and resultant failure of the brittle crust (Schaefer and Kattenhorn, 2004). On Earth these fractures can result in smaller lava flows if the fracture is deep enough to sample the molten interior (Hon et al., 1994).

As mentioned above, there is a strong spatial association between these fractures and the Vinalia Faculae. While the wispy margins of the Vinalia Faculae more closely resemble that of pyroclastic deposits rather than lava flows, this is not unexpected. On Ceres, any flows erupted into the zero-pressure surface environment will boil violently, yielding a deposit more comparable to an explosive deposit similar to pyroclastics (Quick ,2018). Assuming that cryomagmatic fluids utilized the fractures on the lobate flow to reach the surface, the fluids would have evaporated (Ruesch et al., 2018), leaving behind the observed carbonate salts (De Sanctis et al, 2016).

The age of the Occator floor (Neesemann et al.,2018) is such that it is far more likely that the lobate flow is impact melt rather than a lava flow (Scully et al., 2018). However, it seems likely that inflation, and inflation fracturing, of this impact melt crust could still occur if there was cryomagmatic injection from beneath. The distinct composition of the Vinalia deposits (De Sanctis et al, 2016) supports the idea that a subsurface sodium-carbonate bearing cryomagma lies beneath this region of Occator.

One Vinalia Facula is associated with concentric fractures at the base of the crater wall (Fig. 7b). Explosive pyroclasic deposits have been associated with this type of fracture in lunar FFCs, when the underlying magma utilizes the fracture to travel to the surface (Jozwiak et al., 2015). Similar utilization of the Ceres fractures could lead to an explosive deposit of carbonate salts, as discussed for the faculae on the lobate flow. Indeed, cryomagma trav-

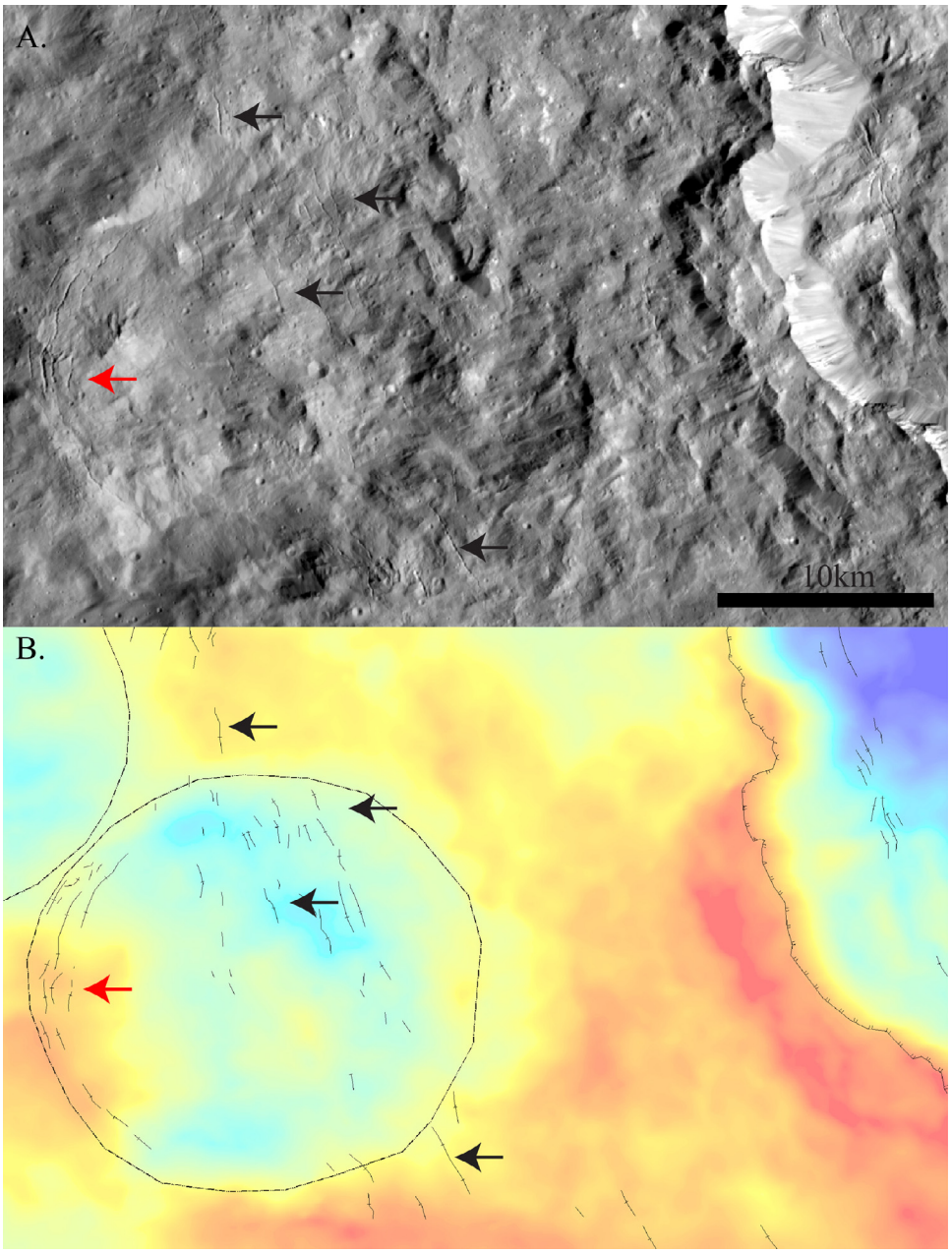

Fig. 9. Circumferential fractures in the crater ejecta. A) LAMO (35 m/pixel) clear filter image of ejecta to the west of the crater rim. B) Fracture map of the same area, shown over the LAMO DTM of Occator crater. The majority of the fractures (black arrows) are circumferential to the Occator rim, but a small number of fractures (red arrow) follow the trace of a smaller crater (dashed circle) completely buried by Occator ejecta.

elling from the putative magma chamber beneath Occator along these fractures may even be the source of the cryomagma presumably causing the inflation of the adjacent flow. However, Zolotov (2017) argued that the carbonate material could have been in the crust prior to impact, and it either mobilized when the crust melted upon impact or evolved in a melt reservoir created by the impact.

2.6. Circumferential fractures in the ejecta blanket

2.6.1. Description

Small scale fractures are identified in Occator's ejecta blanket (Fig. 9). Most of these fractures are circumferential to the rim of the crater (Fig. 9, black arrows). However, there is one location in which the fractures suddenly curve into a different arc (Fig. 9, red arrow). The topographic data suggests that there is a completely buried crater in this location (Fig. 9b), and the observed ejecta fractures are following the rim of this smaller crater rim.

2.6.2. Interpretation

On Mars, circular graben can form over the rims of buried impact craters when they are completely covered by a volatile-rich overburden (Buczkowski and Cooke, 2004; Cooke et al., 2011). This assertion was based on the argument by Cartwright and Lonergan (1997) that compaction is a three-dimensional, volumetric contraction, not just a one-dimensional, gravity-driven, vertical process, as it has generally been modeled. This means that in addition to vertical compaction, wet soils shrink horizontally as they dry because the surface tension of the water pulls the grains toward each other. Buczkowski and Cooke (2004) showed that the

horizontal component of volumetric compaction of a cover material over a buried impact crater is resolved as downslope displacement of cover material along buried crater walls. This downslope movement produces zones of concentrated tension that result in fracturing over their rims. Cooke et al. (2011) built on this work to show that similar fracturing can occur over any topographic high that has been completely buried by a volatile rich cover material that is undergoing volumetric compaction.

The observation that some of the circumferential fractures in the Occator ejecta blanket follow buried crater rims, suggests that the ejecta was volatile-rich at the time of emplacement, and has since out-gassed or dessicated during volumetric compaction.

3. Discussion

With several of the Occator fracture sets tied to proposed magmatic upwelling beneath the crater, it becomes necessary to examine whether or not 1) a cryomagma could be upwelling beneath Occator and 2) how much cryomagma would need to be present to result in the observed features. To accomplish this, we examine the magmatic model invoked for the formation of lunar floor-fractured craters (Jozwiak et al., 2015) and adjust it for Ceres conditions.

The lunar magmatic model suggests that any dike propagating toward the surface under an impact crater will encounter the highly fractured region beneath the crater and stall, because of the low density due to brecciation. However, if the driving pressure of the dike exceeds the local lithostatic pressure the dike will begin to propagate laterally, forming a sill. Increased overburden pressure under the crater wall and crater rim will then cause a pinching off and cessation of the lateral propagation, meaning that the sill can only extend to the edges of the crater floor. If the sill continues to fill with magma, it will begin to dome, forming a laccotlith and resulting in increased bending stresses at the uplifted central regions of the crater floor; this should result in fracturing at the crater center (see Fig. 18 in Jozwiak et al., 2015). However, in those craters in which the ratio of the intrusion diameter to the intrusion depth exceeds a critical value the sill will tabularly deform the overlying crater floor. This will localize bending stresses at the periphery of the intrusion, which will result in fracturing on the crater floor at the base of the crater wall (see Fig. 19 in Jozwiak et al., 2015). On the Moon, the underlying magma can utilize these fractures to reach the surface, resulting in mare or pyroclastic deposits on the floors of some lunar floor-fractured craters, such as Oppenheimer and Alphonsus (Jozwiak et al., 2015).

The growth of a vertical intrusion such as a dike is controlled by the magma pressure, the size of the intrusion, and the strength of the crust (Pollard and Johnson, 1973). Jozwiak et al. (2015) noted that to fracture the floor of a crater following the magmatic model, a dike must first be able to propogate from the top of the mantle (the source of the magma) through the crust. This behavior can be expressed as:

$$P_d = \frac{K_c - \left(\left(\pi^{-1} + 0.25\right) * \Delta\rho * g\right)a^{3/2}}{a^{1/2}} \quad (1)$$

where the driving pressure necessary to propogate such a dike $\mathbf{P_d}$ is a factor of the density difference between the host rock and the magma $\boldsymbol{\Delta\rho}$, the fracture toughness of the host rock $\mathbf{K_c}$, the distance the magma has to travel **a**, and the acceleration due to gravity **g**.

Determining the variables in this equation (Table 1) require knowledge about the composition of the Ceres crust and assumptions about the nature of a supposed cerean cryomagma. Analysis of the surface of Ceres with the *Dawn* Visible and Infrared Mapping spectrometer (VIR) have revealed the widespread presence of Mg-serpentine, ammoniated smectite clays, and Ca/Mg-carbonates (De Sanctis et al., 2015). We use this knowledge to determine a range of values for fracture toughness $\mathbf{K_c}$ and crustal density $\boldsymbol{\rho_c}$ (Table 1). For the distance the magma has to travel **a**, we use the value determined by Scully et al. (2017) for the crustal thickness of Hanami Planum rather than the average crustal thickness determined by Emakov et al (2017).

Castillo-Rogez et al. (2018) utilized the De Sanctis et al. (2015, 2016) observations of the Ceres average surface and bright regions to make assumptions as to the evolution of an early ocean in Ceres. They found that upon freezing various salt species precipitated with ice and clathrate hydrates, especially sodium- and ammonium-carbonates and hydrohalite ($NaCl{\bullet}2H_2O$) while residual brines concentrated ammonia and chlorides of sodium and potassium. This is supported by gravity and topography relaxation studies (Ermakov et al., 2017; Fu et al., 2017), which indicate that brines should still be present under the volatile-rich crust, although mixed with silicates in a high viscosity mud. If we assume that these brines represent the source of the cryomagma inferred by Ruesch et al. (2016), then we can use the density range determined for the brine by Castillo-Rogez et al.(2018) to determine the magma density $\boldsymbol{\rho_m}$ (see Table 1).

Using these values for Ceres and Occator crater, we can determine that a magma under Occator crater would need a driving pressure of only 1.7 MPa to erupt on the surface. While this value matches calculations by Quick (2018), it is significantly less than the 20.6 MPa needed for a dike to the reach the surface of the moon (Jozwiak et al., 2015) and about an order of magnitude less than the pressures required for dikes to reach Europa's surface from comparable depths (Fagents, 2003).

As noted above, the magmatic model invokes both bending stresses due to doming and tabular block uplift of the entire crater floor to explain the fractures observed in lunar FFCs. Wichman and Schultz (1996) determined the driving presesures needed for both of these fracture formation mechanisms. They modeled the growth of the laccolith as the flexure of a layered sequence of elastic plates. Such flexure required a driving pressure $\mathbf{P_d}$ of:

$$P_d = \frac{\left(5.33 w_m B T_e^3\right)}{r^4} \quad (2)$$

where $\mathbf{w_m}$ is the intrusion thickness, **B** is the elastic modulus, $\mathbf{T_e}$ is the intrusion depth, and **r** is the intrusion radius. Meanwhile, they also determined that the driving pressure of the block uplift could be expressed as:

$$P_d = w_m(2k/r + Y_m) \quad (3)$$

where **k** is the magma yield strength and $\boldsymbol{\Upsilon_m}$ is magma weight.

Since Occator is a FFC with concentric fractures at the base of the wall, it has presumably undergone block uplift, with its underlying sill extending to the crater rim. Following Jozwiak et al. (2015), the thickness of an intrusion $\mathbf{w_m}$ beneath a floor-fractured crater that has undergone block uplift is taken to be the difference between the actual depth of the crater and the depth the crater should be. Using the depth to diameter ratio determined for the average Ceres crater (Schenk et al., 2016) the depth of a 92 km crater should be 4.6 km. However, the actual measured depth of Occator is 3.5 km. Therefore, the thickness of the intrusion beneath Occator is assumed to be 1.1 km. Based on the timescale for conductive cooling, an intrusion of this size could take ten to hundreds of thousands of years to completely cool, depending on the value assumed for cryomagma/brine thermal diffusivity. Using this value for intrusion thickness in Eq. (3), we can determine that the driving pressure required to create the block uplift observed at Occator would be 0.33–0.38 MPa.

According to Jozwiak et al. (2015) the depth of the magmatic intrusion is effectively the same as the elastic thickness of the overburden. Therefore, the depth of the putative sill beneath Occator can also be determined by adapting Eqs. (2) and (3) to solve for

Table 1
Variables used to determine the depth of the magmatic intrusion beneath Occator crater.

Symbol	Definition	Assumed value	Source
Ceres properties			
g	Ceres gravitational acceleration	0.28 m/s^2	
ρ_c	Density of Ceres crust	$1254^{-39}{}_{+56}$ kg/m^3	Ermakov et al. (2017)
a	Thickness of Ceres crust	$41^{-4.7}{}_{+3.2}$ km	Ermakov et al. (2017)
Properties of Ceres crustal materials			
K_{IC}	Fracture toughness		
	smectite	0.1–0.8 MPa $m^{1/2}$	Soundararajah et al. (2009)
	carbonate	0.39–0.47 MPa $m^{1/2}$	Al-Shayea and Abduraheem (2001)
E	Young's modulus		
	smectite	0.5–3.5 GPa	Soundararajah et al. (2009)
	carbonate	5.46 GPa	Madhubabu et al. (2016)
	serpentine	35 GPa	Christensen (1966)
ν	Poisson's ratio		
	carbonate	0.36	Madhubabu et al. (2016)
	serpentine	0.34	Christensen (1966)
B	Elastic Modulus ($B = E/(1-\nu)$)		
	carbonate	8.53 GPa	Derived
	serpentine	53.03 GPa	Derived
Properties of Ceres cryomagma/mud ocean			
Υ_m	Magma Weight ($\Upsilon_m = \rho g$)	288.4 kg/m^2s^2	
ρ_m	Density of the Ceres mud ocean brine (cryomagma)	1040–1070 kg/m^3	Castillo-Rogez et al.(2018)
k	Magma yield strength	10^4 Pa	Johnston and Montési, 2017
Properties of Occator crater			
a_H	Thickness of crust at Hanami	58 km	Scully et al. (2017)
w_m	Thickness of Occator intrusion	1.1 km	See text
r	Radius of Occator intrusion	46 km	See text

T_e:

$$T_e^3 = \frac{(2k/r + Y_m) * r^4}{5.33 * B}$$

The elastic modulus of the crust **B** is determined for the range of values assumed by the prevalent minerals found in the Ceres crust; this yields only small variations in the solution of the depth of the intrusion $\mathbf{T_e}$. We use the density range determined for the brine by Castillo-Rogez et al.(2018) to determine the magma weight $\boldsymbol{\Upsilon_m}$. In addition, its intrusion radius **r** for any floor fractured crater would be the radius of the crater floor, which is 46 km for Occator. We determine that the putative sill beneath Occator crater would be 2.9–3.1 km beneath the floor of the crater.

4. Conclusions

A morphologic and structural analysis has been performed to determine how the many fractures associated with Occator might have formed. This analysis suggests that the concentric and radial fractures around the central pit and the concentric fractures high on the crater wall, near the crater rim, most likely formed soon after the crater was formed, due to well known impact cratering processes. However, the concentric floor fractures at the base of the crater wall, and the roughly associated cross-cutting fractures in the lower part of the southwestern wall could have formed due to uplift of the crater floor caused by magmatic injection beneath the crater. A mathematical analysis shows that a cryomagmatic plume (diapir) could have both reached the height necessary to cause fracturing within Occator, but also that the stresses required are reasonable. The linear fractures that extend from the cross-cutting set toward the central pit are most likely just fractures radial to both the southern dome and the central pit reaching each other and linking. However, the linear fractures associated with the Vinalia Faculae seem to have formed due to the expansion from beneath of the lobate flow that they are found on. Finally, the circumferential fractures surrounding Occator appear to have formed due to the volumetric compaction of the ejecta blanket over the buried pre-existing topography.

Acknowledgements

We thank an anonymous reviewer for their comments and suggestions. Support of the Dawn Instrument, Operations, and Science Teams is gratefully acknowledged. This work is supported by grants from NASA through the Dawn project (DLB, JECS, LQ, JCR, PMS, RSP, CAR and CTR were funded from the NASA Dawn project), and from the German Aerospace Center (DLR) (FP and RJ were funded by the German Aerospace Center (DLR)).

Supplementary materials

Supplementary material associated with this article can be found, in the online version, at doi:10.1016/j.icarus.2018.05.012.

References

Al-Shayea, N.A.K.Khan, Abduraheem, A., 2001. Fracture toughness vs. tensile strength for reservoir rocks from Saudi Arabia. In: Sijing, W., Bingjun, Fu, Zhonkui, L. (Eds.), Frontiers of Rock Mechanics and Sustainable Development in the 21st Century. Swets & Zeitlinger Publishers, Netherlands, pp. 169–172.

Bosak, P., Jaros, J., Spudil, J., Sulovsky, P., Vaclavek, V., 1998. Salt plugs in the Eastern Zagros, Iran: results of regional geological reconnaissance. Geolines 7 (1), 3–180.

Bray, V.J., Schenk, P.M., Melosh, H.J., Morgan, J.V., Collins, G.S., 2012. Ganymede crater dimension – implications for central peak and central pit formation and development. Icarus 217, 115–129.

Buczkowski, D.L., Schmidt, B., Williams, D.A., Mest, S.C., Scully, J.E.C., Ermakov, A.E., Preusker, F., Schenk, P., Otto, K., Hiesinger, H., O'Brien, D., Marchi, S., Sizemore, H., Hughson, K., Chilton, H., Bland, M., Byrne, S., Schorghofer, N., Platz, T., Jaumann, R., Roatsch, T., Sykes, M.V., Nathues, A., De Sanctis, M.C., Raymond, C.A., Russell, C.T., 2016. The geomorphology of Ceres. Science 353. doi:10.1126/science.aaf4332.

Buczkowski, D.L., Cooke, M.L., 2004. Formation of double-ring circular grabens due to volumetric compaction over buried impact craters: implications for thickness and nature of cover material in Utopia Planitia, Mars. J. Geophys. Res. 109, E02006. doi:10.1029/2003JE002144.

Cartwright, J.A., Lonergan, L., 1997. Seismic expression of layerbound fault systems of the Eromanga and North Sea Basins. Explor. Geophys., 28 323–331.

Castillo-Rogez, J., Neveu, M.N., Ermakov, A.I., King, S.D., Raymond, C.A., 2018. Chemical differentiation in large icy bodies - Application to Ceres and Europa. Differentiation: Building the Internal Architecture of Planets (LPI Contrib. No. 2084) abs. 4029.

Christensen, N.I., 1966. Elasticity of ultrabasic rocks. J. Geophys. Res. 71 (24), 5921–5931.

Collins, G.S., 2014. Terraced crater wall (mass wasting). Encyclopedia of Planetary Landforms. pubs. Springer Science doi:10.1007/978-1-4614-9213-9_361-1.

Cooke, M.L., Islam, F., McGill, G., 2011. Basement controls on the scale of giant polygons in Utopia Planitia, Mars. J. Geophys. Res. 116. doi:10.129/2011JE003812.

De Sanctis, M.C., Ammanito, E., Raponi, E., Marchi, S., McCord, T.B., et al., 2015. Ammoniated phyllosilicates with a likely outer solar system origin on (1) Ceres. Nature 528, 241–244. doi:10.1038/nature16172, pmid: 26659184.

De Sanctis, M.C., Raponi, A., Ammannito, E., Ciarniello, M., Toplis, M.J., McSween, H.Y., Castillo-Rogez, J.C., Ehlmann, B.L., Carrozzo, F.G., Marchi, S., Tosi, F., Zambon, F., Capaccioni, F., Capria, M.T., Fonte, S., Formisano, M., Frigeri, A., Giardino, M., Longobardo, A., Magni, G., Palomba, E., McFadden, L.A., Pieters, C.M., Jaumann, R., Schenk, P., Mugnuolo, R., Raymond, C.A., Russell, C.T., 2016. Bright carbonate deposits as evidence of aqueous alteration on (1) Ceres. Nature 536, 54–57. doi:10.1038/nature18290.

Dundas, C.M., Mellon, M.T., McEwen, A.S., Lefort, A., Keszthelyi, L.P., Thomas, N., 2008. HiRISE observations of fractured mounds: possible martian pingos. Geophys. Res. Letts. 35, L04201. doi:10.1029/2007GL031798.

Ermakov, A.I., Fu, R.R., Castillo-Rogez, J.C., Raymond, C.A., Park, R.S., Preusker, F., Russell, C.T., Smith, D.E., Zuber, M.T., 2017. Constraints on Ceres' internal structure and evolution from its shape and gravity measured by the Dawn spacecraft. J. Geophys. Res. 122, 2267–2293. doi:10.1002/2017JE005302.

Fagents, S.A., 2003. Considerations for effusive cryovolcanism on Europa: the post Galileo perspective. J. Geophys. Res. 108, 5139. doi:10.1029/2003JE002128.

French, B.M., 1998. Traces of Catastrophe: A Handbook of Shock-Metamorphic Effects in Terrestrial Meteorite Impact Structures. LPI Contribution No. 954.

Fu, R.R., Ermakov, A., Marchi, S., Castillo-Rogez, J.C., Raymond, C.A., Hager, B.H., Zuber, M.T., King, S.D., Bland, M.T., De Sanctis, M.C., Preusker, F., Park, R.S., Russell, C.T., 2017. Interior structure of the dwarf planet Ceres as revealed by surface topography. Earth Planet. Sci. Letts. 46, 153–164. doi:10.1016/j.epsl.2017.07.053.

Greeley, R., Fink, J.H., Gault, D.E., Guest, J.E., 1982. Experimental simulation of impact cratering on icy satellites. In: Morrison, D. (Ed.), Satellites of Jupiter. University Of Arizona Press, Tucson, pp. 340–378.

Hiesinger, H.S.Marchi, Schmedemann, N., Schenk, P., Pasckert, J.H., Neesemann, A., O'Brien, D.P., Kneissl, T., Ermakov, A.I., Fu, R.R., Bland, M.T., Nathues, A., Platz, T., Williams, D.A., Jaumann, R., Castillo-Rogez, J.C., Ruesch, O., Schmidt, B., Park, R.S., Preusker, F., Buczkowski, D.L., Russell, C.T., Raymond, C.A., 2016. Cratering on Ceres: Implications for its crust and evolution. Science 353. doi:10.1126/science.aaf4759.

Hon, K., Kauahikaua, J., Denlinger, R., MacKay, K., 1994. Emplacement and inflation of pahoehoe sheet flows: observations and measurements of active lava flows on Kilauea volcano, Hawaii. GSA Bull. 106, 351–370.

Jaumann, R., Preusker, F., Krohn, K., von der Gathen, I., Stephan, K., Matz, K.-D., Elgne, S., Otto, K., Schmedemann, N., Neesemann, A., Roatsch, T., Kersten, E., Schroeder, S., Schulzeck, F., Tosi, F., De Sanctis, M.C., Buczkowski, D., Scully, J.E.C., Hiesinger, H., Raymond, C., Russell, C.T., Stein, N.T., Williams, D.A., Ruesch, O., Schenk, P., 2017. Topography and geomorphology of the interior of Occator crater on Ceres. Lunar Planet. Sci. Conf. XLVIII abs. 1440.

Johnston, S.A., Montési, L.G.J., 2017. The impact of a pressurized regional sea or global ocean on stresses on Enceladus. J. Geophys. Res. Planets 122. doi:10.1002/2016JE005217.

Jozwiak, L.M., Head, J.W., Wilson, L., 2015. Lunar floor-fractured craters as magmatic intrusions: geometry, modes of emplacement, associated tectonic and volcanic features, and implications for gravity anomalies. Icarus 248, 424–447. doi:10.1016/j.icarus.2014.10.052.

Jozwiak, L.M., Head, J.W., Zuber, M.T., Smith, D.E., Neumann, G.A., 2012. Lunar floor-fractured craters: Classification, distribution, origin and implications for magmatism and shallow crustal structure. J. Geophys. Res. 117. doi:10.1029/2012JE004134.

Krohn, K., Jaumann, R., Stephan, K., Otto, K.A., Schmedemann, N., Wagner, R.J., Tosi, K.-D.Matz,F., Zambon, F., von der Gathen, I., Schulzeck, F., Schröder, S.E., Buczkowski, D.L., Hiesinger, H., McSween, H.Y., Pieters, C.M., Preusker, F., Roatsch, T., Raymond, C.A., Russell, C.T., Williams, D.A., 2016. Cryogenic flow features on Ceres: implications for crater-related cryovolcanism. Geophys. Res. Letts. 43. doi:10.1002/2016GL070370.

Li, J.Y., McFadden, L.A., Parker, J.W., Young, E.F., Stern, S.A., Thomas, P.C., Russell, C.T., V.Sykes, M., 2006. Photometric analysis of 1 Ceres and surface mapping from HST observations. Icarus 182, 143–160. doi:10.1016/j.icarus.2005.12.012.

Madhubabu, N., Singh, P.K., Kainthola, Ashutosh, Mahanta, Bankim, Tripathy, A., Singh, T.N., 2016. Prediction of compressive strength and elastic modulus of carbonate rocks. Measurement 88, 202–213. doi:10.1016/j.measurement.2016.03.050.

Moore, J.M., Malin, M.C., 1988. Dome craters on Ganymede. Geophys. Res. Lett. 15, 225–228.

Nathues, A., Hoffmann, M., Schaefer, M., Le Corre, L., Reddy, V., Platz, T., Cloutis, E.A., Christensen, U., Kneissl, T., Li, J.-Y., Mengel, K., Schmedemann, N., Schaefer, T., Russell, C.T., Applin, D.M., Buczkowski, D.L., Izawa, M.R.M., Keller, H.U., O'Brien, D.P., Pieters, C.M., Raymond, C.A., Ripken, J., Schenk, P.M., Schmidt, B.E., Sierks, H., 2015. Sublimation in bright spots on (1) Ceres. Nature 528, 237–240. doi:10.1038/nature15754, pmid: 26659183.

Neesemann, et al., 2018. (this issue), The various ages of Occator crater, Ceres: Results of a comprehensive synthesis approach. Icarus.

Neveu, M., Desch, S.J., 2015. Geochemistry, thermal evolution, and cryovolcanism on Ceres with a muddy ice mantle. Geophys. Res. Lett. 42. doi:10.1002/2015GL066375, 10,197-10,206.

Preusker, F., Scholten, F., Matz, K.-D., Elgner, S., Jaumann, R., Roatsch, T., Joy, S.P., Polanskey, C.A., Raymond, C.A., Russell, C.T., 2016. Dawn at Ceres - Shape model and rotational state. Lunar Planet. Sci. Conf. XLVII abs.1954.

Pollard, D.P., Johnson, A.M., 1973. Mechanics of growth of some laccolithic intrusions in the Henry Mountains, Utah. II. Bending and failure of overburden layers and sill formation. TectonoPhys. 18, 311–354.

Quick, L.C., 2018. (this issue), A possible brine reservoir beneath Occator crater: thermal and compositional evolution and formation of the Ceralia dome and the Vinalia Faculae. Icarus.

Ruesch, O., Platz, T., Schenk, P., McFadden, L.A., Castillo-Rogez, J.C., Byrne, S., Preusker, F., O'Brien, D.P., Schmedemann, N., Williams, D.A., Li, J.-Y., Bland, M.T., Hiesinger, H., Sykes, M.V., Kneissl, T., Neesemann, A., Schaefer, M., Nathues, A., Roatsch, T., Pasckert, J.H., Schmidt, B., Hoffmann, M., Buczkowski, D.L., Raymond, C.A., Russell, C.T., 2016. Cryovolcanism on Ceres. Science 353. doi:10.1126/science.aaf4286.

Ruesch, O., Quick, L.C., Landis, M., Sori, M., Čadek, O., Brož, P., Otto, K., Bland, M.T., Byrne, S., Castillo-Rogez, J.C., Hiesinger, H., Jaumann, R., Krohn, K., McFadden, L.A., Nathues, A., Neesemann, A., Preusker, F., Roatsch, T., Schenk, P.M., Scully, J., Sykes, M.V., Williams, D.A., Raymond, C.A., Russell, C.T., 2018. Bright carbonate surfaces on Ceres as remnants of salt-rich water fountains. Icarus doi:10.1016/j.icarus.2018.01.022.

Russell, C.T., Raymond, C.A., 2011. The Dawn mission to Vesta and Ceres. Space Sci. Rev. 163, 3–23. doi:10.1007/s11214-011-9836-2.

Schaefer, C.J., Kattenhorn, S.A., 2004. Characterization and evolution of fractures in low-volume pahoehoe lava flows, eastern Snake River Plain, Idaho. GSA Bull. 116. doi:10.1130/B25335.2.

Schenk, P.M., 1993. Central pit and dome craters: exposing the interiors of Ganymede and Callisto. J. Geophys. Res. 98, 7475–7498.

Schenk, P., Marchi, O'Brien, D.P., Bland, M., Platz, T., Hoogenboom, T., Kramer, G., Schröder, S., de Sanctis, M., Buczkowski, D., Sykes, M., McFadden, L.A., Ruesch, O., Le Corre, L., Schmidt, B., Hughson, K., Russell, C.T., Scully, J., Raymond, C., 2016. Impact cratering on the small planets Ceres and Vesta: S–C transitions, central pits and the origin of bright spots. Lunar Planet. Sci. Conf. XLVII abs. 2697.

Schenk, et al., 2018. (this issue) The central pit and dome at cerealia facula bright deposit and floor deposits in occator crater, Ceres: morphology, comparisons and formation. Icarus.

Schultz-Ela, D.D., Jackson, M.P.A., Vendeville, B.C., 1993. Mechanics of active salt diapirism. Tectonophysics 228, 275–312.

Schultz, P.M., 1976. Floor-fractured lunar craters. Moon 15, 241–273. doi:10.1007/BF00562240.

Scully, J.E.C., Buczkowski, D.L., Schmedemann, N., Raymond, C.A., Castillo-Rogez, J.C., King, S.D., Bland, M.T., Ermakov, A.I., O'Brien, D.P., Marchi, S., Longobardo, A., Russell, C.T., Fu, R.R., Neveu, M., 2017. Evidence for the interior evolution of Ceres from geologic analysis of fractures. Geophys. Res. Letts. 44, 9564–9572. doi:10.1002/2017GL075086.

Scully, J.E.C., Buczkowski, D.L., Raymond, C.A., Neesemann, A., Bowling, T., Schenk, P.M., Williams, D.A., Castillo-Rogez, J.C., Russell, C.T., 2018. Ceres' Occator crater and its faculae explored through geologic mapping. Icarus doi:10.1016/j.icarus.2018.04.014.

Sierks, H., et al., 2011. The Dawn Framing Camera. Space Sci. Rev. 163, 263–328. doi:10.1007/s11214-011-9745-4.

Sims, D.W., Morris, A.P., Wyrick, D.Y., Ferrill, D.A., Waiting, D.J., Franklin, N.M., Colton, S.L., Umezawa, Y.T., Takanashi, M., Beverly, E.J., 2013. Analog modeling of normal faulting above Middle East domes during regional extension. Amer. Assc. Petroleum Geol. Bull. 97, 877–898.

Stein, N.T., Ehlmann, B.L., Palomba, E., De Sanctis, M.C., Nathues, A., Hiesinger, H., Ammannito, E., Raymond, C.A., Jaumann, R., Longobardo, A., Russell, C.T., 2017. Icarus doi:10.1016/j.icarus.2017.10.014.

Soundararajah, Q.Y., Karunaratne, B.S.B., Rajapakse, R.M.G., 2009. Montmorillonite polyaniline nanocomposites: Preparation, characterization and investigation of mechanical properties. Mat. Chem. Phys. 113, 850–855. doi:10.1016/j.matchemphys.2008.08.055.

Tornabene, L.L., et al., 2007. Impact melting and the role of subsurface volatiles: Implications for the formation of valley networks and phyllosilicate-rich lithologies on early Mars. Seventh International Conference on Mars abs. 3288.

Wichman, R.W., Schultz, P.H., 1996. Crater-centered laccoliths on the Moon: Modeling intrusion depth and magmatic pressure at the crater Taruntius. Icarus 122, 193–199.

Wood, C.A., Head, J.W., Cintala, M.J., 1978. Interior morphology of fresh martian craters: The effects of target characteristics. Lunar Planet. Sci. 9, 3691–3709.

Zolotov, M.Y., 2017. Aqueous origins of bright salt deposits on Ceres. Icarus 296, 289–304. doi:10.1016/j.icarus.2017.06.018.